



AC electrical properties of transition metal dichalcogenide based polypyrrole composites

Anegundi Sunilkumar¹ · Shidiginamola Manjunatha² · Yaled Thippeswamy Ravikiran³ · Sabu Thomas⁴ · Teluguru Machappa¹

Received: 26 December 2022 / Accepted: 11 April 2023 / Published online: 25 April 2023
© Institute of Chemistry, Slovak Academy of Sciences 2023

Abstract

Tantalum disulphide (TaS₂) embedded polypyrrole (PPy) composites in varied compositions have been prepared by the chemical polymerization technique. PPy and PPy/TaS₂ composites were subjected to scanning electron microscopy (SEM), energy dispersive X-ray spectroscopy (EDX), transmission electron microscopy (TEM) and selected area electron diffraction (SAED) to understand their morphology. X-ray diffraction (XRD) and fourier transform infrared spectroscopy (FTIR) studies were carried out to account for their structural properties. Room temperature AC conductivity of these composites has been studied in the frequency range between 50 Hz to 5 Mhz. AC conductivity of the composites showed increasing trend with increasing wt% of TaS₂- which can be explained on the basis of hopping of polarons. Conductivity of PPy/TaS₂-50 wt% composite has shown conductivity of $4.6 \times 10^{-3} \text{ Scm}^{-1}$ at 100 Hz as compared to those of other composites. Dielectric response of these composites has been explained using Maxwell–Wagner polarization, and the tangent loss curves have been understood based on the Rezlescu model. These composites can be considered in the design of low and mid frequency devices.

Keywords Polypyrrole · Tantalum disulphide · Composite · AC conductivity · Dielectric behaviour

Introduction

Polymers in general have many applications but conducting polymers (CPs) have very attractive future in terms of the technological applications that they are being used for wide range of fields (Pongali Sathya Prabu et al. 2021). These polymers, which have a framework of π -conjugated polymer chains, allow for the delocalization of easily available

π electrons, giving them distinctive electrical properties. (Gunjal et al. 2023; Manjunatha et al. 2021) In the past few decades, the CPs viz. polythiophene, polypyrrole, polyaniline, and polyphenylene have been extensively studied by doping them with different metal oxides, semiconductors, metalloids and sulphides. (Ćirić-Marjanovic 2013; Megha et al. 2020a; Vinay et al. 2019) Advanced research in the area of conducting polymers has led to a number of applications in areas such as super capacitors, (Tu et al. 2018) drug delivery, light emitting devices, (Tessler et al. 1996) rechargeable batteries and sensors (Machappa and Badrunnisa 2021; Chethan et al. 2020; Kushwaha et al. 2022). Amongst the abovementioned CPs, PPy has emerged as the most appealing material due to its unique transport feature, along with the ease of synthesis, good electrical capabilities and outstanding research potential (Sunilkumar et al. 2019a).

Composites of PPy with ZnO, (Chougule et al. 2012) PbTiO₃, (Basavaraja et al. 2007) MgFe₂O₄, (Megha et al. 2017a) Y₂O₃, (Vishnuvardhan et al. 2006) Fe₂O₃, (Suri et al. 2002) MWCNT, (Wu et al. 2009) Graphite oxide, (Gu et al. 2009) WO₃, (Zhu et al. 2010) have been synthesized and their electrical transport properties are observed to be very interesting. Composites and blends formed out

Anegundi Sunilkumar and Shidiginamola Manjunatha have contributed equally.

✉ Yaled Thippeswamy Ravikiran
ytrcta@gmail.com

¹ Department of Physics, VTURC, Ballari Institute of Technology and Management, Ballari, Karnataka 583104, India

² V.V. Sangha's Independent PU College, Ballari, Karnataka 583104, India

³ Department of PG Studies & Research in Physics, Government Science College, Chitradurga, Karnataka 577501, India

⁴ School of Energy Materials, Mahatma Gandhi University, Kottayam, Kerala 686560, India

of PPy have found vivid applications in the areas of sensors, super capacitors, solar cells, paints, gas sensing, electromagnetic shielding, inks and light emitting diodes. (Das et al. 2012; Aguiar et al. 2021)

Current research trends, apart from metal oxide-based PPy composites, transition metal dichalcogenides (TMDs) have received a lot of attention. CPs and TMDs can together form a unique class of hybrid materials (Manjunatha et al. 2018a, 2018b). Amongst all TMDs, MoS₂, WS₂ have been studied extensively along with conducting polymers. But TaS₂ which has a larger electropositivity compared to other TMDs possess unique properties that need to be investigated with the conducting polymers (Manjunatha et al. 2019a). TaS₂ which has more surface energy due to the fact that the surface charge of TaS₂ increases due to the van der Waals gaps between its 2D-layers which favours the optimal synergy when combined with CPs. High electrical conductivity of TaS₂ has drawn the attention of researchers to explore its interesting electrical transport properties (Chamlagain et al. 2017). A recent study in PPy/WS₂ composites has revealed that the AC conductivity has increased significantly and it has better humidity sensing properties compared to the pristine PPy (Sunilkumar et al. 2021, 2019b). Our earlier research that showed an improvement in the humidity sensing properties of polyaniline/ TaS₂ and PPy/ TaS₂ composites has prompted us to explore the AC electrical transport properties of PPy/TaS₂ composites (Sunilkumar et al. 2019a; Manjunatha et al. 2019a).

In view of the above discussion, we present here the synthesis of PPy and PPy/TaS₂ composites by chemical polymerization technique and results related to their structure using XRD, FTIR, SEM, TEM and EDAX techniques. Room temperature AC electrical and dielectric properties of PPy and PPy/TaS₂ composites as a function of frequency have been studied thoroughly.

Experimental

Materials and methodology

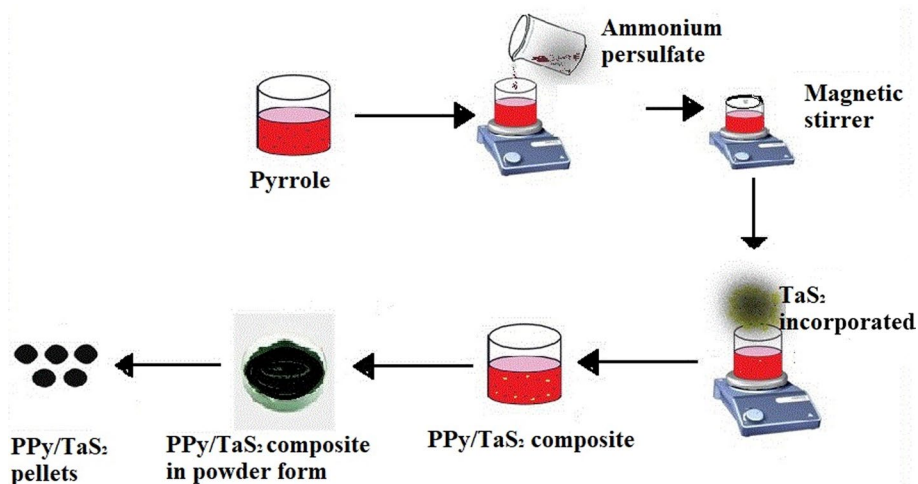
Analytical grade reagents such as pyrrole [C₄H₄NH], ammonium per sulphate [(NH₄)₂S₂O₈] were obtained from SD fine chemicals, Mumbai, India. TaS₂ was procured from Alfa Aesar.

0.03 M solvent of double distilled pyrrole monomer was taken in a beaker and using a magnetic stirrer, it was stirred to stir for 30 min. Tantalum disulphide powder, in the weight ratios 10, 30, 50wt%, were finely ground and added separately to a beaker containing pyrrole by continuous stirring. Then, 0.06 M of ammonium persulphate was progressively added drop by drop to the pyrrole solution using a burette. Complete reaction took about 5–6 h under uninterrupted conditions with continuous stirring. Precipitate of the above mixtures was filtered and repeatedly washed with acetone and distilled water to obtain PPy/TaS₂ composites. Composites were then dried in an oven at 100°C till weight consistency was achieved. Pristine PPy was prepared in an analogous procedure without TaS₂. A schematic procedure for the synthesis of PPy/TaS₂ composites is illustrated in Fig. 1.

Characterization

Characterization is an important aspect in analysing the samples in every field of research. Characterization of pristine PPy and PPy/TaS₂ composites was carried out using the techniques viz. scanning electron microscopy (SEM), energy dispersive X-ray spectroscopy (EDX), transmission electron microscopy (TEM), selected area electron diffraction (SAED), X-ray diffraction (XRD), fourier transform infrared spectroscopy (FTIR).

Fig. 1 Schematic illustration of formation of PPy/TaS₂ composites

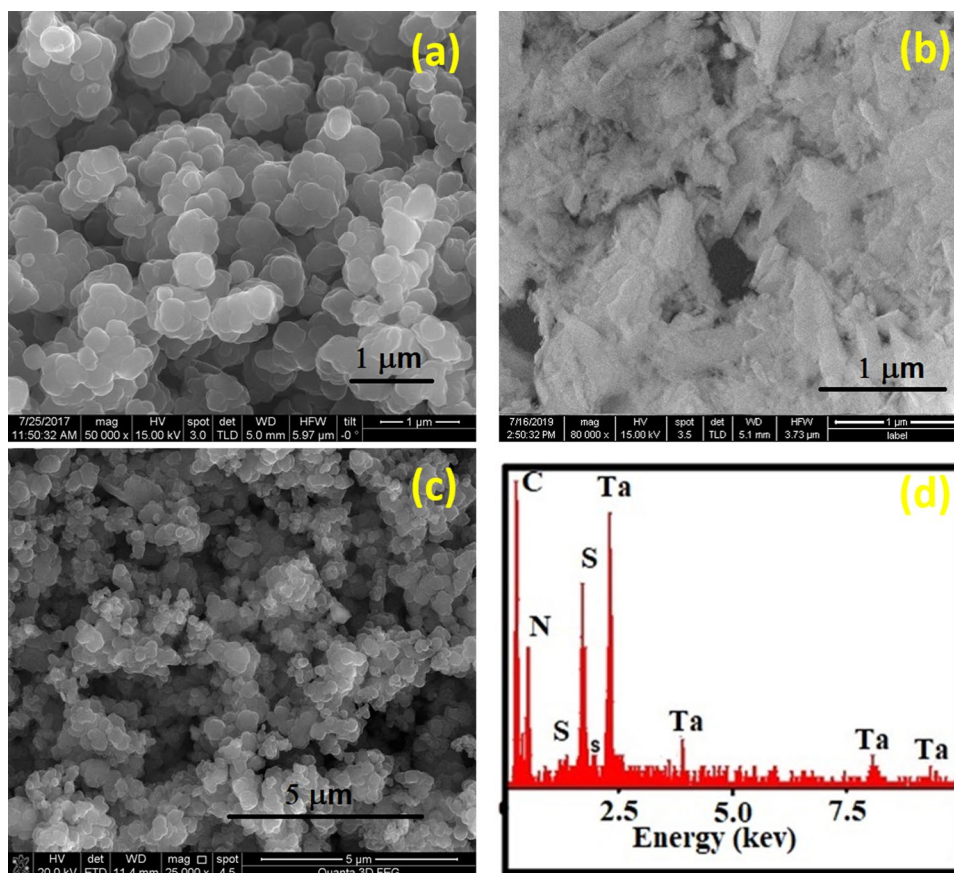


PPy, TaS₂ and PPy/TaS₂ composites were subjected to a Bruker D8 Advance X-ray diffractometer to obtain the XRD spectra. The source for X-ray used was copper K α with wavelength 1.541 Å, and the scanning was performed in the range 10°–80° of 2 θ at a rate of 1.1° min⁻¹. FTIR spectra of the present composites were obtained from a Frontier PerkinElmer FTIR tool with 4 cm⁻¹ resolution, with 16 number of scans and for the wavenumber range 450–4000 cm⁻¹. A Quanta 3D FEG and FEI Nova Nano SEM 600 instruments were used to capture the SEM photographs. For the EDX, a EDAX genesis instrument was employed. Similarly, a TEM, JEOL-3010 instrument was used to capture the TEM images of the present composites.

AC response measurements

Room temperature AC response measurements in the frequency range between 50 Hz to 5 Mhz were made on the present composites. Powdered composites were formed into the pellet form with the help of a hydraulic press. The thickness and diameter of the obtained pellets were measured to be around 1.5 mm and 10 mm, respectively. To establish the ohmic contacts, both the major surfaces of the pellets have been silver coated.

Fig. 2 SEM images of **a** PPy, **b** TaS₂, **c** PPy/TaS₂-50% composite and **(d)** EDX spectra for PPy/TaS₂-50% composite



Results and discussion

FESEM

Figure 2 shows the SEM images of PPy, TaS₂ and PPy/TaS₂-50 wt% composite. The surface morphology from image of PPy (Fig. 2a) indicates that the distribution is of uniform polymeric morphology. This is in accordance with the typical spheroid particle which is a distinctive and signature morphology for CPs. Figure 2b reveals the SEM image of pure tantalum disulphide showing the continuous 2D TaS₂ sheets. SEM image of the composite as shown in Fig. 2c reveals that TaS₂ sheets have been distributed uniformly in PPy matrix. Change in structure of the composite has resulted in electron delocalization which brings about an enhancement in the electrical conducting properties (Megha et al. 2018). Figure 2d depicts the EDX spectrum of the composite PPy/TaS₂-50%. This spectrum confirms the existence of peaks belonging to the elements such as nitrogen, carbon, oxygen, the basic entities of PPy and also the peaks related to sulphur and tantalum in tantalum disulphide.

Grain sizes of PPy and the composite were obtained using image-J software and the corresponding histograms in Fig. 3 reveal the number frequency versus the grain sizes. Mean

grain size of PPy and the composite were determined to be 0.54 μm and 0.42 μm , respectively. It is evident from the histograms that the decrease in grain size in the composite compared to PPy, has enhanced the grain boundaries leading to the decrease in inter-granular distance. This reduced inter-granular distance favours easier charge transport through the polymer chains (Megha et al. 2020a).

TEM

Figure 4a depicts the transmission electron micrograph of PPy/TaS₂-30wt% composite with high resolution image and SAED pattern of the composite. Dark region of the image unveils TaS₂ and light region indicates the PPy matrix. The image clearly exhibit that TaS₂ has confined in PPy chain matrix with clear encapsulation of TaS₂ in PPy. Figure 4b depicts the SAED picture of the composite exhibiting the crystalline nature of the composite as similar to our earlier studies (Manjunatha et al. 2018a, 2019b). PPy/TaS₂-30wt% composite exhibited crystalline nature as confirmed by the

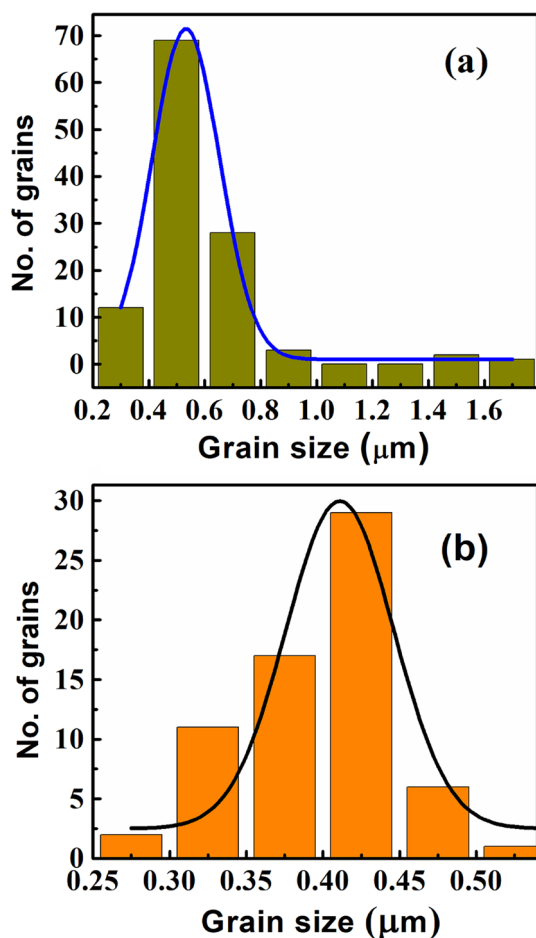


Fig. 3 Particle size histograms depicting the number frequency versus size distribution of **a** PPy and **b** PPy/TaS₂-50% composite

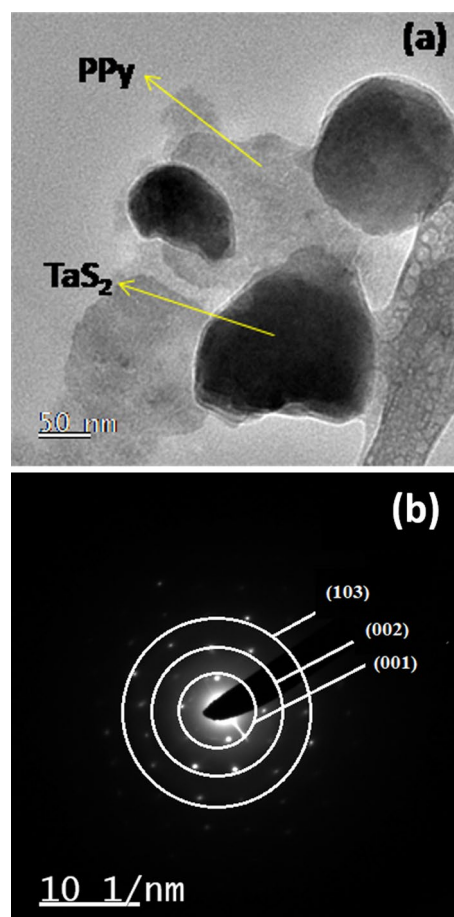


Fig. 4 **a** High Resolution TEM image of the PPy/TaS₂-50% composite, **b** Selected Area Electron Diffraction pattern

diffraction spots obtained from the selected area electron diffraction which is well in agreement with that of the results obtained from the XRD pattern of the composite.

XRD

Figure 5 depicts the XRD spectra of pure PPy, TaS₂ and PPy/TaS₂-30 wt% composites along with the assignment of hkl values. Figure 5a shows X-ray diffraction peaks of TaS₂ with assigned planes. The data support the hexagonal crystal structure with trigonal prismatic coordination in the 2H phase (Manjunatha et al. 2019a) which is established from search match software bearing the JCPDS file No. 02–0137. Figure 5b displays the XRD pattern of pristine polypyrrole with a broad hump at around $2\theta = 24.77^\circ$. This broad peak manifests the amorphous nature and the short range chain order of polypyrrole (Allen et al. 1997). Figure 5c depicts the XRD pattern of PPy/TaS₂-50% composite which display the peaks of PPy and TaS₂ substantiating the monotonous dispersion of TaS₂ in PPy matrix (Sakthivel and Boopathi 2014).

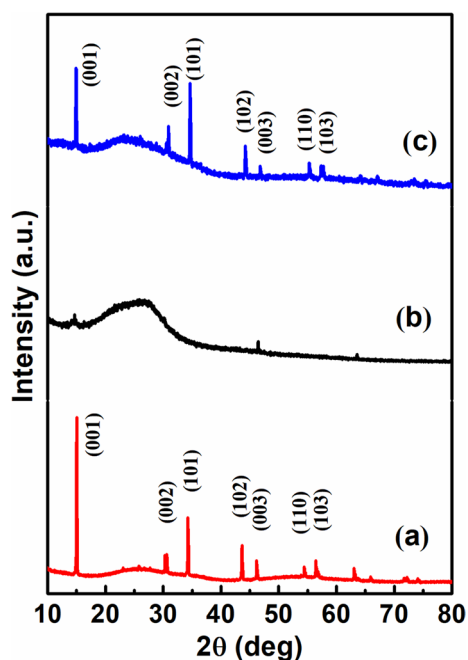
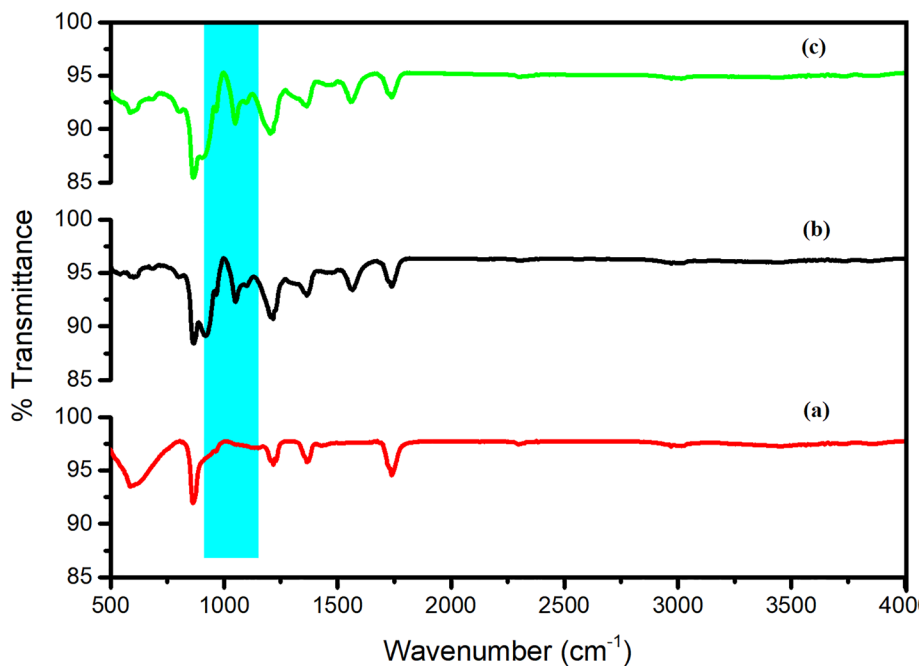


Fig. 5 XRD spectrum for **a** TaS₂, **b** PPy and **c** PPy/TaS₂-50% composite

FTIR

FTIR spectra for TaS₂, Ppy and composite PPy/TaS₂-50 wt% are displayed in Fig. 6. The bands at 587 and 862 cm⁻¹ in the FTIR spectra of TaS₂ (Fig. 6a) have been ascribed to the tantalum–sulphur stretching vibrations and sulphur–sulphur stretching vibrations (Liang and Andrews 2002). FTIR spectrum of pure PPy (Fig. 6b) exhibits the characteristic bands

Fig. 6 FTIR spectra of **a** TaS₂, **b** PPy and **c** PPy/TaS₂-50% composite



at 919, 1050, and 1217 cm⁻¹, which can be, respectively, attributed to the C–H wagging, C–N stretching, and C–H deformation vibrations of PPy. The stretching vibrations of C–N, C–C, C–H, and N–H in the pyrrole ring (Fig. 6c) correspond to the bands at 1366, 1566, 2971 and 3896 cm⁻¹ (Mane et al. 2015). Characteristic absorption bands of PPy and TaS₂ with slight displacement hint at a well-established development in the composite. Also, the band at 1050 cm⁻¹ corresponds to the characteristic charge delocalization band. This band in the composite has found to be with higher % transmittance indicating the increase in delocalization of π -electrons in the polymer chains of the composite and thus resulting in higher conductivity of the composite. (Megha et al. 2020b)

AC response

The frequency dependent AC conductivity of PPy and the composites with 10, 30 and 50 wt% is presented in Fig. 7. Within the studied range of composition and frequency, order of the AC conductivity was measured to be in the range 10⁻²–1 S cm⁻¹. It can be noted from Fig. 7 that the AC conductivity of the composites exhibits a frequency independent behaviour up to a certain frequency, called as critical frequency, f_c . Beyond this frequency, AC conductivity is frequency dependent—as it shoots up sharply with the applied AC frequency. The critical frequencies have increased with increasing weight percent of composites. Frequency independent conductivity and frequency dependent conductivities are, respectively, ascribed to short and long range, back and forth motion of charge carriers (Megha et al. 2020b). Conductivities above the critical frequency

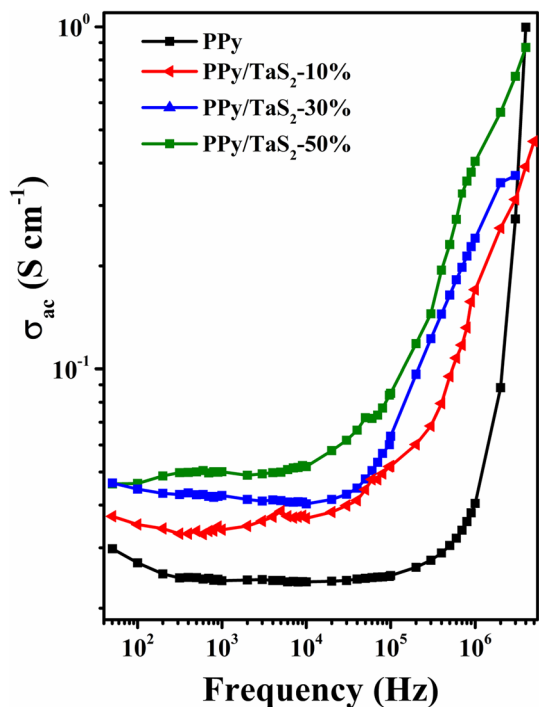


Fig. 7 Frequency dependence of AC conductivity for PPy and its composites

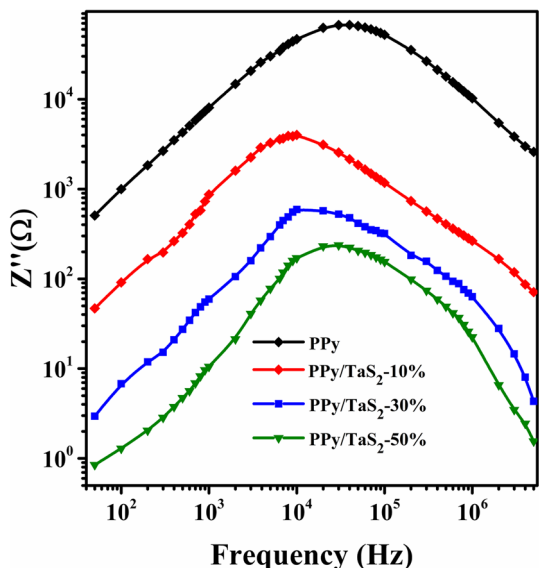


Fig. 8 Variation of imaginary part of impedance of PPy and PPy/TaS₂ composites with frequency

were used to evaluate the power law index using least square linear regression method, and the values were found to be in the range of 0.3–1.

From Fig. 7, it can also be pointed out that the conductivity of the composites was higher than PPy. This has been attributed to the decreased inter-chain separation due to the

incorporation of tantalum disulphide into PPy matrix. This results in creation of more defects which in turn generates higher number of polarons (Bisquert and Belmonte 2004). These polarons can now hop on to longer distances in PPy chain matrix. Conductivity of the composites with wt% 10, 30 and 50 was found to be increasing and it was found to be highest for 50 wt% composite. The polarization of charge carriers enhanced the conductivity of composites than that of the pure polypyrrole. Incorporation of tantalum disulphide into PPy matrix has resulted in the polarization of charge carriers at the specified localized sites, which in turn has led to the increase in conductivity of the composites.

Figure 8 reveals the variation of imaginary part of impedance of PPy and PPy/TaS₂ composites with frequency. The overall behaviour of all the composites reveals the relaxation in the system (Li et al. 2016a). As we increase the weight%, the relaxation peak shifts towards the higher frequency side. The relaxation time was calculated by using the formula $\tau = \frac{1}{2\pi f_p}$. Here, f_p represents the frequency of peak position of the plot. For PPy, the relaxation time was determined to be 3.9 μ s, whereas in case of the PPy/TaS₂-50% composite, the relaxation time was found to be in the range 1.9 μ s. As the value of relaxation time decreases hopping length of charge carriers also decreases- leading to the increase in conductivity of the composite (Sunilkumar et al. 2021).

Figure 9 depicts the variation of dielectric constant with frequency for PPy and the composites. The dielectric constant was found to decrease with increase in frequency. The dielectric constant was found to be high at lower frequencies in all the samples. This has been ascribed to the hopping of charge carriers (Megha et al. 2017b). Hopping of charge carriers cause polarisation in dielectric materials at higher frequencies, resulting in lower dielectric constant values. With the constrained mobility of bound carrier dipoles, the space charge polarisation occurs resulting in orientation polarisation, which may be the cause for the dielectric constant to drop with the increase in applied frequency (Maity et al. 2015).

From Fig. 9, it can also be observed that the dielectric constant decreases for PPy compared to the PPy/TaS₂ composites. Initially, for 10 wt%, the dielectric constant was measured to be high and with increasing concentration of TaS₂, the dielectric constant decreased linearly. From 10 to 1000 kHz, a sudden decline in the value of ϵ' was noticed, which can be explained by space charge effects and interfacial polarisation effects. The charge carriers produced by the Maxwell–Wagner–Sillars polarisation effect are stored in the components' interfacial area. In this two-phase model, the interfacial polarisation of charge carriers is present in the low frequency region due to imperfect formation of layers in the composite which in turn electrically conductive and so dielectric relaxation response of the material causes

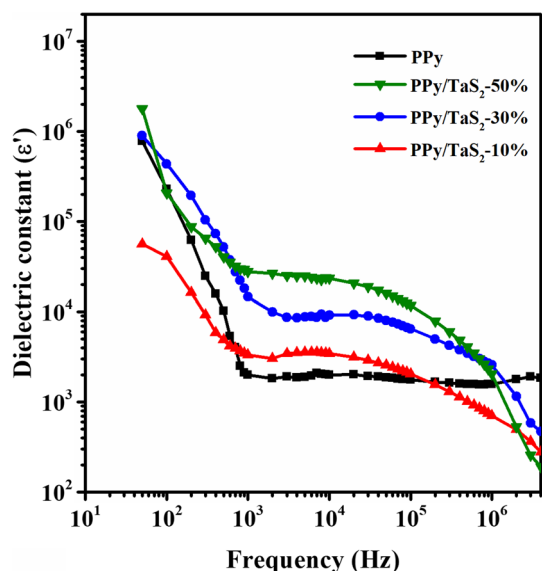


Fig. 9 Frequency variation of real dielectric constant for PPy and PPy/TaS₂ composites

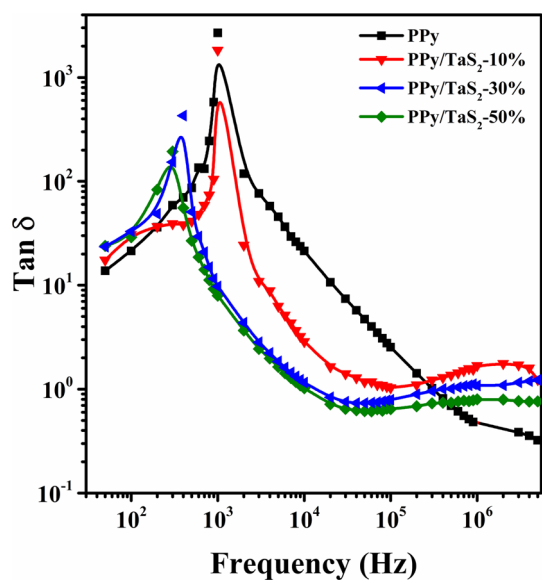


Fig. 10 Frequency dependence of dielectric loss tangent for PPy and PPy/TaS₂ composites

the drop in ϵ' at higher frequencies. The delayed molecular polarisation that occurs within the external applied field is responsible for the dielectric relaxation (Li et al. 2016b).

Variation of dielectric loss tangent with frequency in pristine PPy and its composites is shown in Fig. 10. Usually, the dielectric loss tangent occurs in the form of heat due to movement of charge carriers in the material. In Fig. 10, it can be observed that the dielectric loss tangent curve exhibits an unusual behaviour by marking a peak for all the composites. This peak is referred to as the dielectric relaxation

peak following the Rezlescu model (Megha et al. 2019). In the present composites, the dielectric relaxation peaks were found to be in the frequency range 10^3 – 10^4 Hz. When the frequency of the polarons and the frequency of the applied AC field match with each other, a resonance phenomenon occurs resulting in the appearance of dielectric relaxation peak (Sadiq et al. 2015). The materials exhibiting higher dielectric loss at lower frequencies can be explored for applications such as medium frequency devices.

Conclusions

PPy/TaS₂ composites have been synthesized by using chemical polymerization method. PPy composited with TaS₂ manifests an increment in AC conductivity with increasing wt % of TaS₂ in the composites. PPy/TaS₂-50wt% composite has shown the maximum conductivity amongst all the prepared composites due to hopping of charge carriers and same can be evidenced from impedance studies. The composites have also exhibited enhanced conducting properties than that of pure polypyrrole. The dielectric constant and dielectric loss can be understood by Rezlescu and Maxwell–Wagner model. The present composites exhibiting higher dielectric loss at lower frequencies can be explored for their potential applications in the development of medium frequency devices. Further, these conducting polymer-transition metal dichalcogenides composites have been planned for studying their gas sensing behaviour to encash their unique electrical properties.

Acknowledgements All the authors acknowledge the support received from JNCASR, Bengaluru, for providing the experimental facilities for various characterization techniques.

Declarations

Conflict of interest The authors declare that they have no conflict of interest.

References

- Allen NS, Murray KS, Fleming RJ, Saunders BR (1997) Physical properties of polypyrrole films containing trisoxalatometallate anions and prepared from aqueous solution. *Synth Met* 87:237–247
- Basavaraja C, Choi YM, Park HT, Huh DS, Lee JW, Revanasiddappa M, Raghavendra SC, Khasim S, Vishnuvardhan TK (2007) Preparation, characterization and low frequency ac conduction of polypyrrole-lead titanate composites. *Bull Korean Chem Soc* 28:1104–1108
- Bisquert J, Belmonte GG (2004) Interpretation of AC conductivity of lightly doped conducting polymers in terms of hopping conduction*. *Russ J Electrochem* 40:352–358
- Chamlagain B et al (2017) Thermally oxidized 2D TaS₂ as a high- κ gate dielectric for MoS₂ field-effect transistors. *2D Mater* 4:031002-1-031002-8. <https://doi.org/10.1088/2053-1583/aa780e>

- Chethan B, Prakash HGR, Ravikiran YT, Kumari SCV, Manjunatha S, Thomas S (2020) Humidity sensing performance of hybrid nanorods of polyaniline-Yttrium oxide composite prepared by mechanical mixing method. *Talanta* 215:120906. <https://doi.org/10.1016/j.talanta.2020.120906>
- Chougule MA, Dalavi DS, Patil PS, Moholkar AV, Agawane GL, Kim JH, Sen S, Patil VB (2012) Novel method for fabrication of room temperature polypyrrole – ZnO nanocomposite NO₂ sensor. *Measurement* 45:1989–1996. <https://doi.org/10.1016/j.measurement.2012.04.023>
- Ćirić-Marjanovic G (2013) Recent advances in polyaniline composites with metals, metalloids and nonmetals. *Synth Met* 170:31–56. <https://doi.org/10.1016/j.synthmet.2013.02.028>
- Das TK, Prusty S, Das TK, Prusty S (2012) Review on conducting polymers and their applications. *Polym Plast Technol Eng* 51:1487–1500. <https://doi.org/10.1080/03602559.2012.710697>
- de Aguiar MF, Leal ANR, de Melo CP, Alves KGB (2021) Polypyrrole-coated electrospun polystyrene films as humidity sensors. *Talanta* 234:122636. <https://doi.org/10.1016/j.talanta.2021.122636>
- Gu Z, Zhang L, Li C (2009) Preparation of highly conductive polypyrrole/graphite oxide composites via in situ polymerization. *J Macromol Sci* 48:1093–1102. <https://doi.org/10.1080/00222340903035576>
- Gunjaj LB, Manjunatha S, Chethan B, Nagabhushana NM, Ravikiran YT, Machappa T, Thomas S (2023) Humidity sensing performance of polyaniline - neodymium oxide composites. *MRS Commun.* <https://doi.org/10.1557/s43579-023-00336-3>
- Kushwaha CS, Singh P, Shukla SK (2022) Transition Metal and Conducting Polymers Nanocomposite for Sensing of Environmental Gases. In: *Metal Nanocomposites for Energy and Environmental Applications*. pp 471–487
- Li H, Tan Y, Liu P, Guo C, Luo M, Han J, Lin T, F. Huang MC, (2016a) Atomic-sized pores enhanced electrocatalysis of tas2 nanosheets for hydrogen evolution. *Adv Mater* 28:8945–8949. <https://doi.org/10.1002/adma.201602502>
- Li H, Tan Y, Liu P, Guo C, Luo M, Han J, Lin T, Huang F, Chen M (2016b) Atomic-sized pores enhanced electrocatalysis of TaS₂ nanosheets for hydrogen evolution. *Adv Mater* 28:8945–8949. <https://doi.org/10.1002/adma.201602502>
- Liang B, Andrews L (2002) Infrared spectra and density functional theory calculations of group V transition metal sulfides. *J Phys Chem A* 106:3738–3743. <https://doi.org/10.1021/jp013790n>
- Machappa T, Badrunnisa S (2021) Sodium metavanadate dispersed in Polyaniline composite matrix film for sensing application. *J Polym Res* 28:1–12. <https://doi.org/10.1007/s10965-021-02734-4>
- Maity N, Kuila A, Das S, Mandal D, Shit A, Nandi AK (2015) Optoelectronic and photovoltaic properties of graphene quantum dot-polyaniline nanostructures. *J Mater Chem A* 3:20736–20748. <https://doi.org/10.1039/C5TA06576C>
- Mane AT, Navale ST, Pawar RC, Lee CS, Patil VB (2015) Microstructural, optical and electrical transport properties of WO₃ nanoparticles coated Polypyrrole hybrid nanocomposites. *Synth Met* 199:187–195
- Manjunatha S, Machappa T, Sunilkumar A, Ravikiran YT (2018a) Tungsten disulfide: an efficient material in enhancement of AC conductivity and dielectric properties of polyaniline. *J Mater Sci Mater Electron* 29:11581–11590. <https://doi.org/10.1007/s10854-018-9255-1>
- Manjunatha S, Chethan B, Ravikiran YT, Machappa T (2018b) Room temperature humidity sensor based on polyaniline- tungsten disulfide composite. *AIP Conf Proc* 1953:030096-1-030096-4. <https://doi.org/10.1063/1.5032431>
- Manjunatha S, Machappa T, Ravikiran YT, Chethan B, Sunilkumar A (2019a) Polyaniline based stable humidity sensor operable at room temperature. *Phys B Condens Matter* 561:170–178. <https://doi.org/10.1016/j.physb.2019.02.063>
- Manjunatha S, Machappa T, Ravikiran YT, Chethan M, Revanasiddappa M (2019b) Room temperature humidity sensing performance of polyaniline – holmium oxide composite. *Appl Phys A* 125:361. <https://doi.org/10.1007/s00339-019-2638-1>
- Manjunatha S, Megha R, Chethan B, Prashantkumar M, Ravikiran YT, Machappa T (2021) Structural and AC electrical properties of tantalum disulfide embedded polyaniline composites. *J Mater Eng Perform* 30:1885–1894. <https://doi.org/10.1007/s11665-021-05526-5>
- Megha R, Kotresh S, Ravikiran YT, Ramana CHVV, Kumari SCV, Thomas S (2017a) Study of alternating current conduction mechanism in polypyrrole-magnesium ferrite hybrid nanocomposite through correlated barrier hopping model. *Compos Interfaces* 24:55–68. <https://doi.org/10.1080/09276440.2016.1185298>
- Megha R, Ravikiran YT, Kumari SCV, Chandrasekhar T, Thomas S (2017b) Optimized polyaniline-transition metal oxide composites : a comparative study of alternating current conductivity via correlated barrier hopping model. *Polym Compos* 2012:1–11
- Megha R, Ravikiran YT, Chethan B, Raj Prakash HG, Vijaya Kumari SC, Thomas S (2018) Effect of mechanical mixing method of preparation of polyaniline- transition metal oxide composites on DC conductivity and humidity sensing response. *J Mater Sci Mater Electron.* <https://doi.org/10.1007/s10854-018-8714-z>
- Megha R, Ravikiran YT, Kumari SCV, Prakash HGR, Ramana CVV, Thomas S (2019) Enhancement in alternating current conductivity of HCl doped polyaniline by modified titania. *Compos Interfaces* 26:309–324. <https://doi.org/10.1080/09276440.2018.1499352>
- Megha R, Ravikiran YT, Vijaya Kumari SC, Rajprakash HG, Manjunatha S, Revanasiddappa M, Prashantkumar M, Thomas S (2020a) AC conductivity studies in copper decorated and zinc oxide embedded polypyrrole composite nanorods: interfacial effects. *Mater Sci Semicond Process* 110:104963. <https://doi.org/10.1016/j.mssp.2020.104963>
- Megha R, Ravikiran YT, Kumari SCV, Prakash HGR, Revanasiddappa M, Manjunatha S, Dastager SG, Thomas S (2020b) Structural and electrical characterization studies for ternary composite of polypyrrole. *J Mater Sci Mater Electron* 31:18400–18411. <https://doi.org/10.1007/s10854-020-04386-4>
- Pongali Sathya Prabu N, Madhu Mohan MLN, Pal K (2021) Dielectric responses and stimulative optical shuttering action of self-assembly supramolecular hydrogen bond liquid crystalline formation via x- and y-types benzoic acids. *J Mol Liq* 343:117386. <https://doi.org/10.1016/j.molliq.2021.117386>
- Sadiq I, Naseem S, Naeem Ashiq M, Khan MA, Niaz S, Rana MU (2015) Structural and dielectric properties of doped ferrite nanomaterials suitable for microwave and biomedical applications. *Prog Nat Sci Mater Int* 25:419–424. <https://doi.org/10.1016/j.pnsc.2015.09.011>
- Sakthivel S, Boopathi A (2014) Synthesis and characterization of polypyrrole (PPY) thin film by spin coating technique. *J Chem Chem Sci* 4:150–155
- Sunilkumar A, Manjunatha S, Chethan B, Ravikiran YT, Machappa T (2019a) Polypyrrole – Tantalum disulfide composite: an efficient material for fabrication of room temperature operable humidity sensor. *Sens Actuators A Phys* 298:111593. <https://doi.org/10.1016/j.sna.2019.111593>
- Sunilkumar A, Manjunatha S, Machappa T, Chethan B, Ravikiran YT (2019b) A tungsten disulphide-polypyrrole composite-based humidity sensor at room temperature. *Bull Mater Sci* 42:271. <https://doi.org/10.1007/s12034-019-1955-5>
- Sunilkumar A, Manjunatha S, Ravikiran YT, Revanasiddappa M, Prashantkumar M, Machappa T (2021) AC conductivity and dielectric studies in polypyrrole wrapped tungsten disulphide composites. *Polym Bull.* <https://doi.org/10.1007/s00289-021-03552-w>

- Suri K, Annapoorni S, Sarkar AK, Tandon RP (2002) Gas and humidity sensors based on iron oxide \pm polypyrrole nanocomposites. *Sens Actuators, B Chem* 81(2–3):277–282
- Tessler N, Denton GJ, Friend RH (1996) Lasing from conjugated-polymer microcavities. *Nature* 382:695–697
- Tu CC, Peng PW, Lin LY (2018) Weight ratio effects on morphology and electrocapacitive performance for MoS₂/polypyrrole electrodes. *Appl Surf Sci* 444:789–799
- Vinay K, Revanasiddappa M, Manjunatha S, Shivakumar K, Ravikiran YT (2019) Room temperature humidity sensing behaviour of silver decorated polyaniline composite Room temperature humidity sensing behaviour of silver decorated polyaniline composite. *Mater Res Express* 6:104003
- Vishnuvardhan TK, Kulkarni VR, Basavaraja C, Raghavendra SC (2006) Synthesis, characterization and ac conductivity of polypyrrole/Y₂O₃ composites. *Bull Mater Sci* 29:77–83
- Wu T, Chang H, Lin Y (2009) Synthesis and characterization of conductive polypyrrole/multi-walled carbon nanotubes composites with improved solubility and conductivity. *Compos Sci Technol* 69:639–644. <https://doi.org/10.1016/j.compscitech.2008.12.010>
- Zhu J, Wei S, Zhang L, Mao Y, Ryu J, Mavinakuli P, Karki AB, Young DP, Guo Z (2010) Conductive polypyrrole/tungsten oxide metamaterials with negative permittivity. *J Phys Chem C* 114:16335–16342

Publisher's Note Springer Nature remains neutral with regard to jurisdictional claims in published maps and institutional affiliations.

Springer Nature or its licensor (e.g. a society or other partner) holds exclusive rights to this article under a publishing agreement with the author(s) or other rightsholder(s); author self-archiving of the accepted manuscript version of this article is solely governed by the terms of such publishing agreement and applicable law.